Geometric Calibration of CCD Camera Using Planer Object

Conference Paper · July 1994

CITATIONS
0

READS
14

1 author:

Mohammed Taleb Obaidat
Jordan University of Science and Technology; Jadara University
99 PUBLICATIONS **376** CITATIONS

SEE PROFILE

Geometric Calibration of CCD Camera Using Planar Object

Article *in* Journal of Surveying Engineering · August 1996

DOI: 10.1061/(ASCE)0733-9453(1996)122:3(97)

CITATIONS
10

READS
38

2 authors, including:

Mohammed Taleb Obaidat
Jordan University of Science and Technology; Jadara University
87 PUBLICATIONS **271** CITATIONS

SEE PROFILE

GEOMETRIC CALIBRATION OF CCD CAMERA USING PLANAR OBJECT

By Mohammed Taleb Obaidat[1] and Kam W. Wong,[2] Members, ASCE

ABSTRACT: A method of geometric calibration of charge-coupled device (CCD) vision systems for metric measurement has been developed. The method does not require a special calibration facility or accurately surveyed three-dimensional (3D) control points. It only requires that one stereo pair of images of a planar object be acquired with the CCD camera that is to be calibrated. Using a planar wall constraint as a control, the study identified that a priori knowledge of seven parameters of interior orientation could be used to effectively model the interior geometry of known focal length CCD cameras equipped with zoom lenses. Brick walls provided an excellent calibration source of such a calibration facility, because they can provide a sufficiently large number of well-defined points throughout the stereo images at almost any focal setting. The corners of the bricks and mortar joints might be used as target points. Comparison with laboratory calibration using a 3D test field showed that the method of planar constraint was capable of providing results of comparable accuracy at 10–32 mm variable focal settings lens, and potentially even better results at larger focal settings. A root-mean square (RMS) error of better than ±0.2 pixels was achieved consistently for higher values of focal setting. Using about 40–50 stereo image points, the interior geometry of the CCD camera was effectively modeled. Increasing the number of image points increased the stability of the calibration parameters. The method has the potential to be advantageous in terms of practicality, availability and economy; time saving, and providing a large number of image points.

INTRODUCTION

In applications of close-range photogrammetry both metric and nonmetric cameras are used (Adams 1981; Wiley 1991). Therefore, depending on the required accuracy of the extracted three-dimensional (3D) measurements, the calibration method varies from the simple classical approach to highly refined analytical solution in which both the radial and decentering lens distortions are found. The literature reported four approaches to camera calibration: laboratory calibration; on-the-job calibration; self-calibration; and analytical plumb-line calibration (Fryer 1989). With the exception of the self-calibration method, which has a unique procedure, the other methods require a special calibration facility to be designed. Unfortunately, designing these calibration facilities is time-consuming, costly because they need accurate survey to construct the calibration test field and require periodic maintenance.

Proper calibration of the interior geometry of charge-coupled device (CCD) cameras is the key to computer vision metrology. Laboratory calibration using 3D test fields had clearly demonstrated the potential geometric accuracy of computer vision systems (Faig 1975; Fryer 1989; Wiley 1991). Estimated root-mean square (RMS) errors for each of the three coordinates of ±0.2 to ±0.4 mm have been reported in the literature (Faig 1972; Adams 1981).

[1]Asst. Prof., Dept. of Civ. Engrg., Jordan Univ. of Sci. and Technol., (J.U.S.T.), Irbid, P.O. Box 3030, Jordan.

[2]Prof., Dept. of Civ. Engrg., Univ. of Illinois at Urbana-Champaign, Urbana, IL 61801.

Note. Discussion open until January 1, 1997. To extend the closing date one month, a written request must be filed with the ASCE Manager of Journals. The manuscript for this paper was submitted for review and possible publication on April 25, 1995. This paper is part of the ***Journal of Surveying Engineering***, Vol. 122, No. 3, August, 1996. ©ASCE, ISSN 0733-9453/96/0003-0097–0113/$4.00 + $.25 per page. Paper No. 10627.

Methods have been developed for accurate calibration of vision systems using a 3D test field in a laboratory (Brown 1968; Faig 1975; Fraser and Veress 1980; Adams 1981). However, it is technically difficult to establish and maintain a 3D test field consisting of 30 or more targets whose coordinates must be determined to an accuracy better than ± 0.1 mm. For the calibration of zoom lenses, more than 50 control targets will be needed to provide a sufficiently large number of targets for calibration at the full range of focal settings. In practice, such calibration facilities are available only in a few research laboratories.

The key requirement to extract accurate 3D measurements from vision systems is to perform frequent calibration of the geometric distortion characteristics of the system (Brown 1971; Wolf and Loomer 1975; Fryer 1989; Wiley and Wong 1992). Unlike film-based cameras, CCD cameras have no distortion due to emulsion problems or film buckling (Fraser and Veress 1980; Curry and Baumrind 1986). Sources of geometric distortion include: optical lens distortion, analog-to-digital (A/D) conversion, and electronic effect and sensor stability (El-Hakim 1986; El-Hakim et al. 1989; Beyer 1990; Wiley and Wong 1992). Vision systems calibrations must be able to account for sources of random and systematic errors represented by the radial and the two decentering distortion components, the affine scaling, and the principal point coordinates.

There is a need to develop a method of geometric calibration that can be easily performed by users of CCD vision systems for metric measurement. The method should require no special calibration facility or accurately surveyed 3D control points. This paper reports on the development of a practical and effective calibration method based on the principle of planar constraint. One possible scene is using a brick wall, which is available in most buildings or construction sites, as a calibration field. This can provide an excellent calibration environment for the planar calibration method by using the mortar joints as targets. In fact, this kind of wall is also advantageous for zoom lens applications because it can provide the calibration environment for almost any focal setting.

MATHEMATICAL DEVELOPMENT

The basic concept of the proposed camera calibration scheme is based on the condition that the two bundles of rays from a stereo pair of images acquired by one camera for a planar object must intersect on the plane. Fig. 1 illustrates the geometry of stereo images taken for a planar wall from two different positions acquired with the camera that is to be calibrated. For a fixed focal length, in the complete absence of geometric distortion, two bundles of rays for point J in Fig. 1, representing the two images, would intersect perfectly in space. Thus, the condition of spatial intersection provides the geometric condition to determine geometric distortion in the direction perpendicular to the scan lines, i.e., in the column direction. The planar object provides the additional constraint that all conjugate pairs of rays must intersect at points located on a plane. This second condition provides the geometric constraint for determining the geometric distortions along the direction of the scan lines, i.e., along the row direction.

CONDITION EQUATIONS

Assuming that light rays travel in straight lines, i.e., all the rays entering a camera lens pass through the exposure center, each ray from each camera

J. Surv. Eng. 1996.122:97-113.

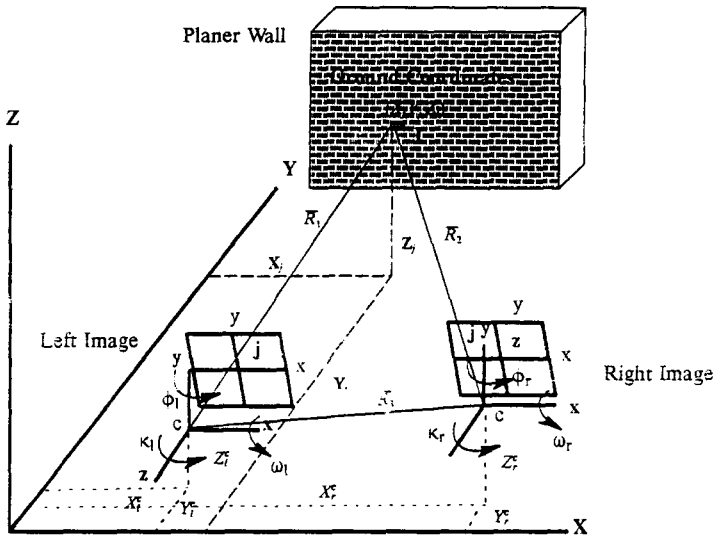

FIG. 1. Enforcing Bundle Rays to Intersect on a Planar Wall

exposure (say the left exposure) has the following transformation equation between photographic coordinates of the image point and the ground coordinates of the corresponding object points:

$$X_j - X_l^c = \lambda_{lj}[m_{11}(x_{lj} - x_p + \Delta x_{lj}) + m_{21}(y_{lj} - y_p + \Delta y_{lj}) + m_{31}(f)] \quad (1)$$

$$Y_j - Y_l^c = \lambda_{lj}[m_{12}(x_{lj} - x_p + \Delta x_{lj}) + m_{22}(y_{lj} - y_p + \Delta y_{lj}) + m_{32}(f)] \quad (2)$$

$$Z_j - Z_l^c = \lambda_{lj}[m_{13}(x_{lj} - x_p + \Delta x_{lj}) + m_{23}(y_{lj} - y_p + \Delta y_{lj}) + m_{33}(f)] \quad (3)$$

In (1)–(3), X_j, Y_j, Z_j = object space coordinates of point J on the planar wall; X_l^c, Y_l^c, and Z_l^c = object space coordinates of the exposure center of the left image; m_{11}–m_{33} = elements of the orientation matrix and functions of the rotation parameters (ω_l, ϕ_l, κ_l); λ_{lj} = scale factor at the left image point j; x_{lj} and y_{lj} = left photo coordinates of the image point j; x_p and y_p = coordinates of the principal points; f = nominal value of the focal length of the camera; and Δx_{lj} and Δy_{lj} = corrections for geometric lens distortion. Similar equations could be written for the right image rays with subscript r.

The following model expresses corrections for systematic errors of the geometric lens distortion of the CCD cameras (Kenefick et al. 1972; Wong 1980):

$$\Delta x_{lj} = \bar{x}_{lj}(L_1 r_{lj}^2 + L_2 r_{lj}^4) + [P_1(r_{lj}^2 + 2\bar{x}_{lj}) + 2P_2\bar{x}_{lj}\bar{y}_{lj}](1 + P_3 r_{lj}^2) \quad (4)$$

$$\Delta y_{lj} = \bar{y}_{lj}(L_1 r_{lj}^2 + L_2 r_{lj}^4) + [P_2(r_{lj}^2 + 2\bar{Y}_{lj}^2) + 2P_1\bar{x}_{lj}\bar{y}_{lj}](1 + P_3 r_{lj}^2) \quad (5)$$

$$\bar{x}_{lj} = (x_{lj} - x_p)(1 + k); \quad \bar{y}_{lj} = (y_{lj} - y_P); \quad r_{lj} = \sqrt{\bar{x}_{lj}^2 + \bar{y}_{lj}^2} \quad (6\text{–}8)$$

where L_1, and L_2 = parameters of radial lens distortions; P_1, P_2, P_3 = parameters of asymmetric distortions; and k = affine scale parameter.

A nominal value of focal length can be used in the mathematical model. The following represent the collinearity condition equations for the left and right rays:

J. Surv. Eng. 1996.122:97-113.

$$F_{\text{LEFT}} = f(x_{lj}, y_{lj}, x_p, y_p, f, k, l_1, l_2, p_1, p_2, p_3, \omega_l, \phi_l, k_l, X_l^c, Y_l^c, Z_l^c) = 0, \text{ left ray} \tag{9}$$

$$F_{\text{RIGHT}} = f(x_{rj}, y_{rj}, x_p, y_p, f, k, l_1, l_2, p_1, p_2, p_3, \omega_r, \phi_r, k_r, X_r^c, Y_r^c, Z_r^c = 0, \text{ right ray} \tag{10}$$

Each object-space point, like J, on the planar object geometry satisfied the plane equation

$$AX_j + BY_j + CZ_j - 1 = 0 \tag{11}$$

where coefficients A, B, C = points where the plane intersects the three axes (X, Y, and Z) in the object space coordinate system.

Substituting the values of the object-space coordinates (X_j, Y_j, Z_j) from the intersection condition of two rays (Wong 1980) into equation 11 yields

$$A\left[\frac{(X_r^c - X_l^c)v_{lj} - (Y_r^c - Y_l^c)u_{lj}}{(v_{rj}u_{lj} - u_{rj}v_{lj})}u_{rj} + X_r^c\right] + B\left[\frac{(X_r^c - X_l^c)v_{lj} - (Y_r^c - Y_l^c)u_{lj}}{(v_{rj}u_{lj} - u_{rj}v_{lj})}v_{rj} + Y_r^c\right] + C\left[\frac{(X_r^c - X_l^c)v_{lj} - (Y_r^c - Y_l^c)u_{lj}}{(v_{rj}u_{lj} - u_{rj}v_{lj})}w_{rj} + Z_r^c\right] - 1 = 0 \tag{12}$$

Assuming an arbitrary coordinate system for the planar object, like the one shown in Fig. 1 with camera base in the X-axis, the exterior orientation parameters of the left camera position with respect to the planar object and the Y and Z coordinates of the right camera can be found using approximate coordinates of one point located at each of the four corners of the plane. Thus, if all the rays are enforced to intersect on the planar object, (12) has only 15 unknowns as follows:

1. Planar object parameters (A, B, and C)
2. Right camera exterior orientation parameters (X_r^c, ω_r, ϕ_r, and k_r)
3. Principal point coordinates (x_p and y_p)
4. Radial distortion parameters (L_1 and L_2)
5. Decentering distortion parameters (P_1, P_2, and P_3)
6. Affine scaling parameter (k)

Since the available CCD cameras were not manufactured with geometric fidelity in mind, three decentering distortion parameters were used to account for a higher degree of lens decentering. Affine scaling may be significant because of expected imperfect sampling clock (Wiley 1991; Ke 1995).

For scale control, at least one line of known length must be known. The distance equation in object space is given by

$$D_{j2-j1} = \sqrt{(X_{j2} - X_{j1})^2 + (Y_{j2} - Y_{j1})^2 + (Z_{j2} - Z_{j1})^2} \tag{13}$$

where D_{j2-j1} = distance in object space between point $j1$ and $j2$.

To keep the mathematical model as general as possible, it is assumed that the unknown parameters have a priori measured values and approximate values. This will contribute to the following:

$$\ddot{V}_{(15,1)} - \dot{\Delta}_{(15,1)} = \ddot{\varepsilon}_{(15,1)} \tag{14}$$

$\ddot{V}_{(15,1)}$, $\Delta_{(15,1)}$, and $\ddot{\varepsilon}_{(15,1)}$ = residuals, corrections, and discrepancies matrices for the unknown parameters.

After linearizing (12) and (13) by Newton's first-order approximation, and assuming that n points from the planar object appear on the pair of stereo images and m measured distances are available on the planar object, the mathematical model can be written in the following matrix form by combining (12), (13), and (14):

$$\begin{bmatrix} \dot{\mathbf{A}}_{(n,4n)} & 0 & 0 \\ 0 & \ddot{\mathbf{A}}_{(m,n)} & 0 \\ 0 & 0 & I_{15,15} \end{bmatrix} \begin{bmatrix} \dot{\mathbf{V}}_{(4n,1)} \\ \ddot{\mathbf{V}}_{(m,1)} \\ \bar{\mathbf{V}}_{(15,1)} \end{bmatrix} + \begin{bmatrix} \dot{\mathbf{B}}_{(n,15)} \\ \ddot{\mathbf{B}}_{(m,15)} \\ -I_{(15,15)} \end{bmatrix} \dot{\Delta}_{(15,1)} = \begin{bmatrix} \dot{\boldsymbol{\varepsilon}}_{(n,1)} \\ \ddot{\boldsymbol{\varepsilon}}_{(m,1)} \\ \bar{\boldsymbol{\varepsilon}}_{(15,1)} \end{bmatrix} \tag{15}$$

where $\dot{\mathbf{A}}$, $\ddot{\mathbf{A}}$ = residual coefficient matrices for stereo image points and measured distance, respectively; $\dot{\mathbf{V}}$, $\ddot{\mathbf{V}}$, $\bar{\mathbf{V}}$ = residual matrices for stereo image points, measured distance, and unknown parameters, respectively; $\dot{\mathbf{B}}$, $\ddot{\mathbf{B}}$ = corrections coefficient matrices for stereo image points and measured distance, respectively; $\dot{\boldsymbol{\varepsilon}}$, $\ddot{\boldsymbol{\varepsilon}}$, $\bar{\boldsymbol{\varepsilon}}$ = discrepancy factor matrices for stereo image points, measured distance, and unknown parameters, respectively; $\dot{\Delta}$ = vector of corrections for unknown parameters; and n and m = number of given stereo image points and measured distances, respectively.

The following compacted symbolic form might also be used:

$$\bar{\mathbf{A}}_{(n+m+15,4n+m+15)}\bar{\mathbf{V}}_{(4n+m+15,1)} + \bar{\mathbf{B}}_{(n+m+15,15)}\dot{\Delta}_{(15,1)} = \bar{\boldsymbol{\varepsilon}}_{(n+m+15,1)} \tag{16}$$

The least-squares solution to this model results in the following normal equation:

$$\bar{\mathbf{B}}^{\mathbf{T}}(\bar{\mathbf{A}}\bar{\mathbf{W}}^{-1}\bar{\mathbf{A}}^{\mathbf{T}})^{-1}\bar{\mathbf{B}}\dot{\Delta} = \bar{\mathbf{B}}^{\mathbf{T}}(\bar{\mathbf{A}}\bar{\mathbf{W}}^{-1}\bar{\mathbf{A}}^{\mathbf{T}})^{-1}\bar{\boldsymbol{\varepsilon}} \tag{17}$$

where $\bar{\mathbf{W}}$ and superscript $\mathbf{T}$ = weight of four corner points and the matrix transpose notation, respectively.

Knowing the approximate coordinates of four corner points on the planar object will determine the following coordinates with respect to the planar object: (1) the approximate location and orientation of the camera; and (2) the planar object parameters.

A weighted least-squares solution such as the CCDCAL program might also be used to obtain approximations for the exterior orientation parameters of the camera (Wiley 1991).

Initial approximations for distortion corrections might be given as zero values. The principal point might also be considered at the center of the image plane.

The corrections of the parameters were continually added to the results after each iteration until the convergence criteria, which is based on standard unit weight value, was reached. This mathematical procedure is common for any weighted least-squares solution and more details could be found in Wong (1980).

SOFTWARE DEVELOPMENT

CCDCAL_PLANE is a program that has been developed to determine the magnitude of various calibration parameters including: (1) optical distortion parameters; (2) principal point coordinates; (3) affine scaling parameter; and (4) exterior orientation parameters for the CCD camera. The algorithm uses a planar object control as a geometric constraint.

A weighted least-squares adjustment solution for a nonlinear function was performed to solve for the unknowns. The least-squares algorithm has the capacity to detect blunder errors for both the image point observations and the known distances. A robust estimator and data snooping algorithm is incorporated into the program. The observations are initialized with equal weight values. On starting the second iteration, the observations are weighted based on their residuals. The larger the residual, the less the weight of the observation. An individual unknown parameter can be fixed by applying a large weight value, i.e., a very small standard deviation.

CCDCAL_PLANE incorporates a knowledge-based system to detect the user faults in case of failure mode. A set of facts rules are provided within the system for guidance, diagnostics, and counseling for data input and data processing.

RESULTS: PLANAR WALL VERSUS LABORATORY 3D CONTROL

Brick walls provided an excellent calibration environment for planar object control. The corners of the bricks and mortar joints provided a large number of well-defined points at almost any focal setting. Furthermore, the approximate coordinates of four corner points can be easily obtained.

When comparing to a 3D control field, the planar wall calibration facility has the following advantages:

1. It provides a sufficiently large number of targets for calibration over the full range of focal settings, overcoming problems associated with a smaller field of view.
2. It does not require accurate surveying.
3. It does not involve the focal length in calibration; this helps overcome the problem of correlation between exterior and interior orientation parameters of calibration when flat control fields are used (Merchant and Tudhope 1989; Wiley 1991).

To check the potential and the effectiveness of the developed CCD camera calibration scheme, it was essential that the interior geometry of the camera be determined throughout different focal settings. Unfortunately, the available CCD cameras had a narrow range of focal settings. The following focal settings were used in this study: 10, 12, 16, 22.5, and 32 mm.

A laboratory 3D control field was used for the comparison of calibration procedures. The field consisted of 55 targets, which were black circles on a white background with dimensions ranging from 3.81 cm (1.5 in.) to 10.16 cm (4 in.). Fig. 2 shows the 3D control field and the planar brick wall facility used for this study.

When a planar wall is used for the control calibration of CCD cameras, the exact nominal value for the focal length is not always known. It is not always known because it requires a 3D calibration control field which is usually impractical. Consequently, another calibration experiment using a planar wall control and an approximate focal length extracted from the camera's focal setting was conducted. For the CCD cameras used in this study, an approximate value of 94 pixels was equivalent to 1 mm of focal setting. This value was based on an intermediate focal length (f = 16 mm), which has been calibrated using the 3D control field. Fig. 3 shows the relationship between the computed focal lengths from lens marking and the focal lengths obtained from a calibration using a 3D control field for different focal settings.

J. Surv. Eng. 1996.122:97-113.

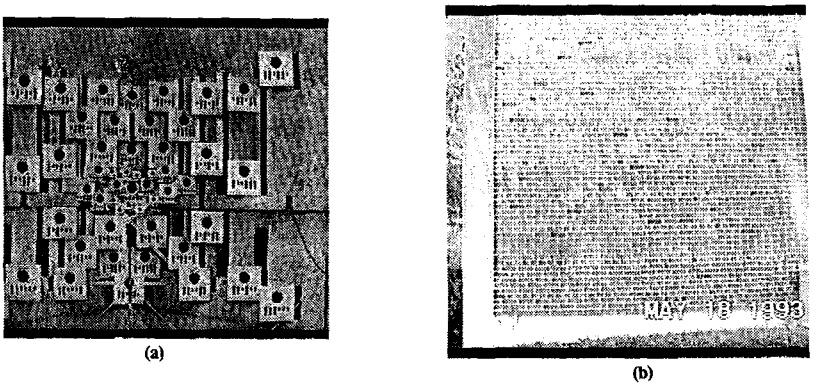

FIG. 2. Laboratory 3D Control Test Field and Planar Wall Control

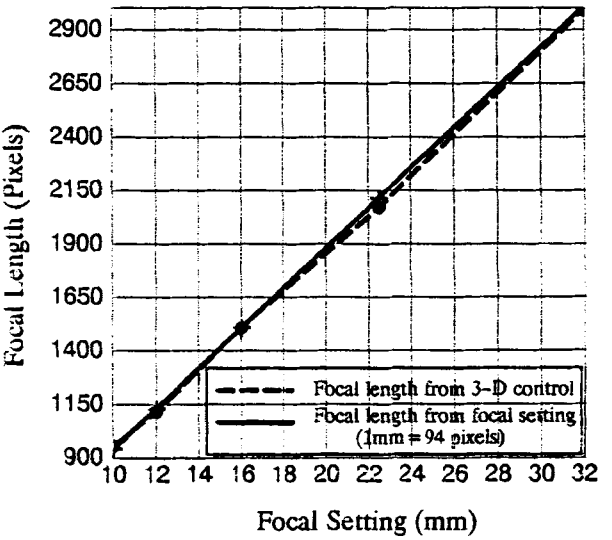

FIG. 3. Calibrated Focal Length (pixels) Using 3D Control Field and Approximate Focal Length from Lens Marking

In the three calibration cases the camera-to-object distance was kept approximately constant for all the focal settings, i.e., the image scale was varied. This distance (approximately equal 7.8 m) was selected based on: (1) the image plane size; (2) the field of view of the available cameras; and (3) the minimum control requirements of the 3D control test field for long focal settings. The base of the camera, in case of the planar wall, was about 1.7 m. The camera had to be moved between the 3D control field and the planar wall for all the focal settings in order to capture calibration images. Although the camera was mounted on a tripod for the purpose of image stability, it was extremely difficult to keep the exact camera configuration and position for all the focal settings. Approximate reproduction of locations and environments were considered sufficient.

Approximations of planar object parameters, and the left and right camera

exposure centers were determined first using the approximate coordinates of four points on the planar object. Then the three rotation parameters were determined. After that, the distortion parameters were modeled. This procedure minimized the negative effects of the small size of the image plane on calibrating the distortion parameters.

The calibration method discussed in Wiley (1991) was used in the 3D control field study for all the focal settings, with the exception that the camera was not kept in the same position during the zoom process due to the aforementioned technical difficulties. The CCDCAL program, which uses automatic target identification, was used for the laboratory calibration procedure to solve for 15 unknowns using the collinearity equations approach (Wiley 1991). The unknowns include (x_p, y_p, f, k, L_1, L_2, P_1, P_2, P_3, X^c, Y^c, Z^c, ω, ϕ, and κ).

The following precautions were taken for calibration images capturing:

1. Warm up the camera and the PC-based vision system for at least 30 min prior to data collection.
2. Maintain a temperature- and humidity-controlled environment for video images of the 3D control field.
3. Use natural sunlight for the planar wall.
4. Minimize the period of time elapsed between capturing the images of the two different cases to avoid the effect of camera stability over time.

The determination of precise calibration parameters requires the user to locate the image points within a certain accuracy. For the planar object calibration, DRSTEREO software package was used to locate the target center to subpixel accuracy by zooming around the target point (Wong and Obaidat 1992). Then, a manual conjugate image point matching might be performed.

CALIBRATION RESULTS

Figs. 4 and 5 show the resultant interior orientation parameters computed for different focal settings for the three different calibration methods. Slight differences were observed between the calibration parameters found using the planar control and those found using the 3D control field. Negligible differ-

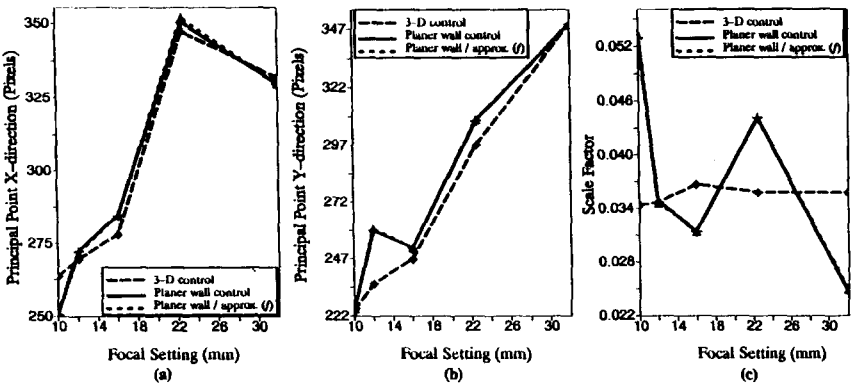

FIG. 4. Principal Point Coordinates (X_p and Y_p) and Scale Factor (K) Calibration Results Using Three Calibration Cases

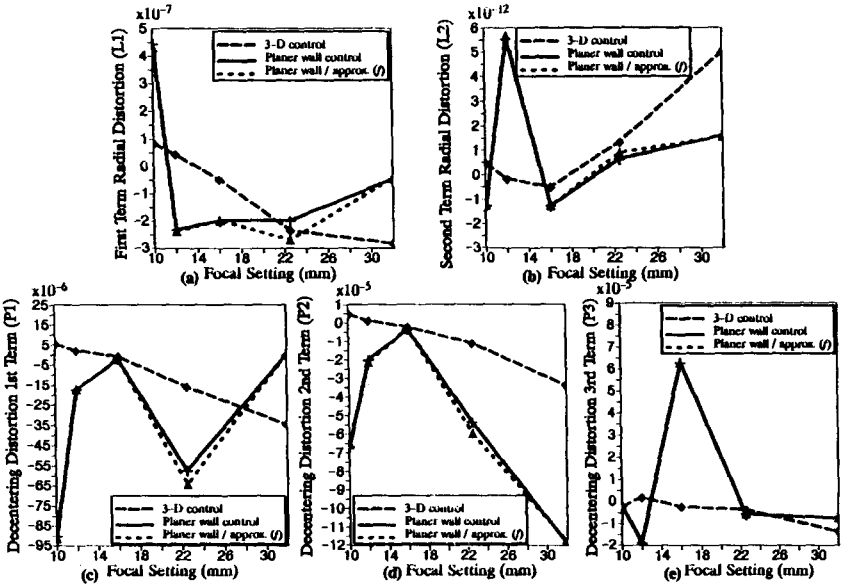

FIG. 5. Calibration Results of Radial and Decentering Distortion Parameters (L_1, L_2, P_1, P_2, and P_3) Using Three Calibration Cases

ences were found between the two cases of planar wall control. In general, for higher focal settings, the standard deviations of principle point coordinates using a planar wall control were smaller than the corresponding standard deviations of 3D control. This gave an indication for precise determination of these calibration parameters. The large number of image points used in the case of the planar wall gave reliable interior orientation parameters even for large focal settings. An approximately linear shift in the principal point location that was directly proportional to the change in the focal length, for the three different calibration cases, was found. This gives an indication of a slight misalignment of the optical axis with respect to the image plane. This result is similar to the results of studies performed by Wiley (1991). Comparable precision was obtained for the parameters of radial and decentering distortion. Nevertheless, comparing the calibration parameters of the different methods is insufficient. Instead, the effectiveness of the calibration method in modeling the interior geometry is the most significant factor for comparing the different calibration methods. This will be studied in the following section.

More precise values were obtained for the X-coordinate of the exposure center and rotation parameters using 3D control. The approximate values of these parameters were first defined in the least-squares solution. For the planar wall, the determination of these values was based on the approximate coordinates of the four corners of the imaged area of the wall, while for the 3D control a direct linear transformation using all the image targets was used. Thus, good approximations for the exterior orientation parameters were obtained using 3D control, while this was not the case for the planar wall.

The standard errors of the exterior orientation parameters increase as the focal setting increases. This is probably due to the smaller image area of both the 3D control field and the planar wall, which act to increase the probability

J. Surv. Eng. 1996.122:97-113.

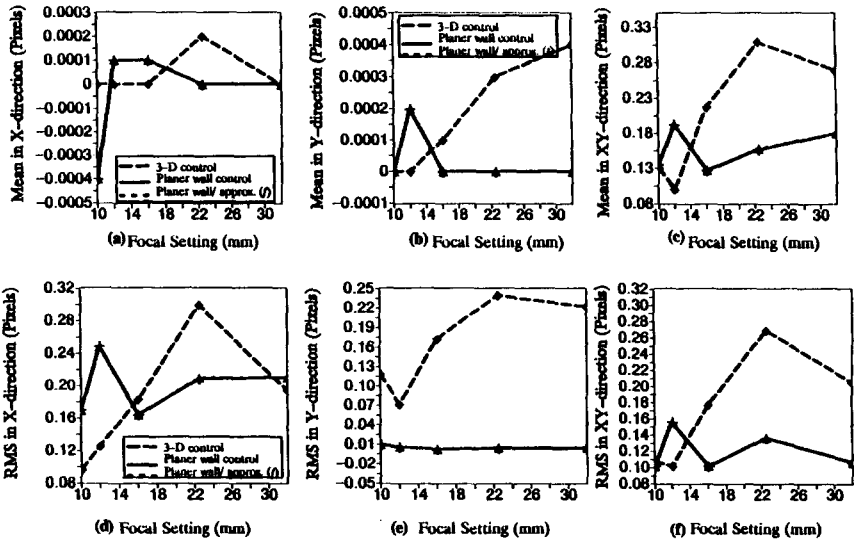

FIG. 6. Mean and RMS Residual Error of Image Coordinates in *X*, *Y*, and XY Vector Directions for Different Focal Settings Using Three Calibration Cases

of errors in the exterior orientation and the planar wall parameters. Although the exterior orientation parameters and the planar object parameters are reported here, they are not the primary objectives of the camera calibration. The radial and decentering distortion parameters, the affine scaling factor, and the principal point coordinates are the important parameters for the camera calibration.

The root-mean square (RMS) residual errors of the image coordinates and their respective mean values are shown in Fig. 6. As expected for random errors, the mean residual errors in the x- and y-directions were about zero. RMS error was smaller in the y-direction than in the x-direction due to the effect of the A/D signal conversion while freezing the image frames using the frame grabber. As the focal length was increased, the value of the RMS of the xy-vector residual error became smaller for the planar wall control than it did for the 3D control. This was not the case for a focal setting of 12 mm, because of the effect of the number of image points. This indicated that the planar wall calibration method was more effective for higher focal setting values, since a large number of image points was available. The superiority and the effectiveness of the planar wall control in modeling distortion in the y-direction was also demonstrated by Fig. 6.

The maximum residual error values for the planar wall are higher than those for the 3D control field. This was a result of the human errors associated with locating the image points manually when using planar wall control, while automatic target centering was done in the case of the 3D control field. Nevertheless, the residual errors as well as the coefficient of variation of the image points residual errors, shown in Fig. 7, showed the potential accuracy and superiority of the planar wall calibration facility over the laboratory 3D control calibration for modeling the interior geometry of the camera (especially for high focal settings).

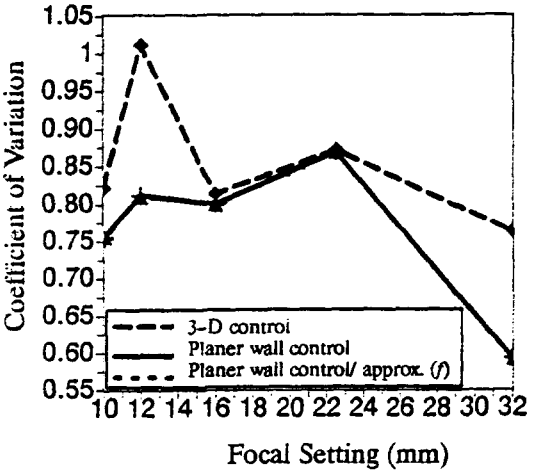

FIG. 7. Coefficient of Variation of Residual Error of Image Coordinates for Different Focal Settings Using Three Calibration Cases

EFFECTIVENESS OF DISTORTION MODEL

Results showed that the correlation between the parameters was almost negligible, indicating that the planar object control calibration method was effective. Although the planar wall calibration facility does not solve for the focal length (which might be considered its major drawback), it minimized the correlation between the parameters. This normally occurred when the weight of the planar wall parameters (A, B, C) was increased, i.e., their precisions were increased. This condition will assure the stability of the planar wall parameters and also establish the exterior orientation parameters of the camera with respect to the planar wall arbitrary coordinate system reference.

Although there were only slight differences between the calibration parameters of a planar wall and a laboratory 3D control, the experimental data showed that using the planar control was much more effective for modeling distortion parameters. Distances were computed using the interior orientation parameters from the 3D control calibration field and the planar wall control approach for different focal settings. The locations of points, for which the distances were computed, were selected far away from the principal points, so that a high distortion effect was expected. Distances were computed with and without distortion corrections for the two calibration cases. Errors were defined as differences between the conventional measurement method and the calculated distances. The focal settings were 10, 12, 16, 22.5, and 32 mm. Pixel sizes on the image domain were 0.821, 0.702, 0.519, 0.378, and 0.216 cm, respectively. The camera was calibrated using various numbers of points for both the 3D control field and the planar wall. The number of points used were 35 and 39, 39 and 38, 37 and 37, 30 and 39, and 16 and 36 points for the 3D calibration field and the planar wall, respectively.

Except for small focal settings, i.e., $f = 10$ and 12 mm, the planar wall control was more effective for recovering the distortion parameters. This was also obvious from the errors in the computed distances and their corresponding relative accuracies (Fig. 8). Of course, the pixel size and the number of points used in the calibration play a major factor in this domain.

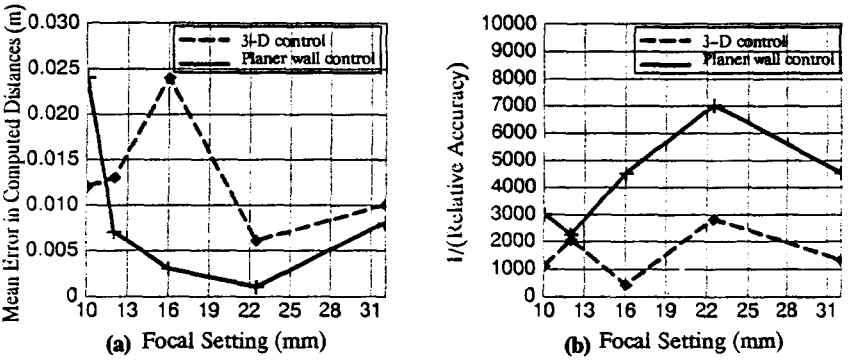

FIG. 8. Errors in Computed Distances on Planar Wall after Applying Distortion Correction Results from both Planar Wall and 3D Control Field

NUMBER OF IMAGE POINTS EFFECT

One of the major advantages of using the planar wall control is that it can provide a sufficiently large number of targets for calibration for a full range of focal settings. Thus, it is worthwhile to study the effect that increasing the number of image points has on the calibration parameters. A moderate focal length, i.e., 16 mm, was used in order to make a compromise between the field of view and effect of planar parameters on calibration results. The image points were evenly distributed on the image domain. Degrees of freedom ranging between 0 and 55 were selected for better representation to study the effect of increasing the number of image points on the calibration parameters.

Fig. 9 shows the effect the number of image points has on the interior orientation parameters. The results show the stability of both the interior and exterior orientation parameters after using a certain number of image points. The larger the number of image points, the more the coplanar rays will be

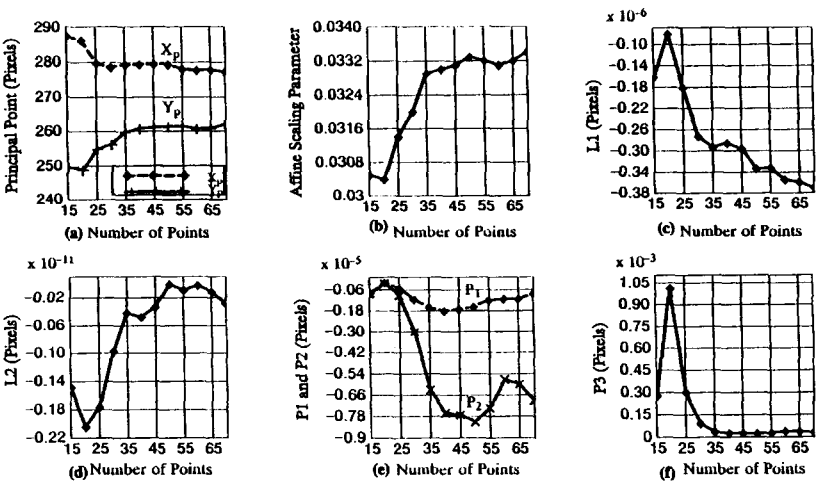

FIG. 9. Changes in Interior Calibration Parameters with Number of Image Points Using Planar Wall as Control (Focal Setting = 16 mm)

enforced to intersect on the planar wall. After a specified number of image points is used, the orientation of the stereo model is complete. Therefore, the calibration parameters become very stable and additional image points have a little effect on them. With the exception of the principal point coordinate in the y-direction (y_p), this reasoning is also supported by the increased precision of the parameters. The parameter standard deviations were becoming smaller. This means that the parameters were becoming more precise. x_p and y_p changed about 10 and 13 pixels, respectively, for a range of 15–70 stereo image points.

The RMS residual error of the image points increased as the number of image points increased, then reached a stable value. The coefficient of variation for image point residuals become better as the number of image points was increased. Fig. 10(a) shows that the coefficient of variation changes with the number of image points. This indicates better calibration modeling of the systematic errors as the number of image points was increased. Another advantage of using a large number of image points is that the number of iterations of the least-squares algorithm will be decreased [Fig. 10(b)]. Consequently, the calibration algorithm time efficiency will be enhanced, although improvements in algorithm efficiency were insignificant compared to the decrease efficiency associated with the acquisition of additional data points.

Since the residual errors of the image points increased as the number of image points increased, it was expected that the computed standard unit weight would increase [Fig. 10(c)]. The mean and RMS of residual errors of

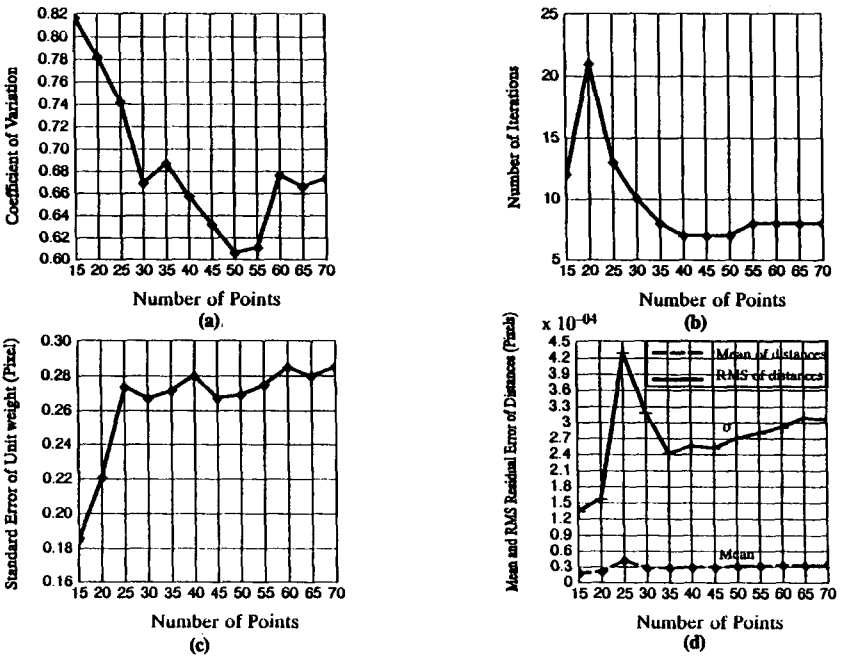

FIG. 10. Number of Image Points Effect on Coefficient of Variation for Residual Error of Image Coordinates for XY Vector, Number of Iterations, Standard Error of Unit Weight, and Mean and RMS Residual Error of Control Distances Using Planar Wall as Control (Focal Length = 16 mm)

J. Surv. Eng. 1996.122:97-113.

the control distances on the planar wall also became stable after a certain number of image points was acquired [Fig. 10(d)].

The general trend of the effect of the number of image points on the calibration parameters is that after a certain number of image points was reached, i.e., around 40–50 points, the interior and exterior orientation parameters and the planar wall parameters became stable. Thus, when the number of image points was increased further, it did not affect the stability of the calibration parameters. Other related literature for using 3D control field indicated that about 50 control targets were needed to provide an acceptable geometrical calibration for distortion model (Faig and Owolabi 1988; Wiley 1991). Numerically, about 50 stereo image points for a planar wall were sufficient to give a good representation for the interior geometry of the CCD cameras.

CONCLUDING REMARKS

A methodology was derived to implement the calibration of CCD cameras, by modeling the passage of light rays through the lens and onto the image plane, using a planar object. A brick wall was used because it could provide an excellent calibration environment for the planar object control. The corners of the bricks and mortar joints provided a large number of well-defined points at almost any focal setting. Furthermore, the approximate coordinates of the planar object and exterior orientation parameters could easily be obtained by using only four corner points.

Comparison with laboratory calibration using a 3D test field showed that the method of planar constraint using a camera with a calibrated focal setting was capable of yielding results of comparable accuracy at 10–32 mm variable focal settings lens. Planar wall calibration with nominal focal length approximated from the lens marking (focal setting) also yielded results similar to that of the calibrated focal length. These results showed the feasibility of calibration using the planar wall facility.

The findings of this study indicated that more accurate calibration can be achieved for larger focal settings using planar wall calibration. This is because the planar wall provided a sufficiently larger number of targets for calibration at the full range of focal settings.

The planar control calibration minimized the correlation between the calibration parameters. This happened because this method does not solve for the focal length.

For larger values of the focal setting, the planar constraint method consistently yielded RMS residual errors of image points to less than 0.2 pixels. Thus, an excellent characterization of the interior geometry was possible.

The maximum errors from planar wall and 3D field calibration were about 0.6 and 0.5 pixels, respectively.

The residual errors as well as the coefficient of variation of the image residual errors showed the potential accuracy and superiority of the planar wall facility calibration over the laboratory 3D control calibration for modeling the interior geometry of the camera in large focal settings. Moreover, experimental results for measuring distances between points showed that planar wall calibration was more efficient in modeling the CCD camera interior geometry.

For evenly distributed image points of the planar object at a certain focal setting, the following observations were made: (1) increasing the number of stereo image points improved the stability and the precision of both the interior and the exterior calibration parameters as well as computational effi-

J. Surv. Eng. 1996.122:97-113.

ciency. However, the total computational time increases; and (2) forty-five to 55 stereo image points were sufficient to model the interior geometry of the CCD cameras.

In conclusion, for the CCD cameras of large focal settings, the planar wall calibration was much more effective than the laboratory 3D calibration field in modeling the systematic errors of the interior geometry. In contrast, a laboratory 3D calibration field has superiority for small focal settings. This result was highly dependent on the image scale and the number of image points used.

ACKNOWLEDGMENTS

The research reported in this paper was conducted as part of the University of Illinois Advanced Construction Technology Center (ACTC) research program sponsored by the U.S. Army Research Office under the DoD-University Research Initiative Program. A full report of this study can be found in Obaidat (1994).

APPENDIX I. REFERENCES

Adams, L. P. (1981). "The use of non-metric cameras in short range photogrammetry." *Photogrammetria*, 36(2), 51–60.

Beyer, H. A. (1990). "Line jitter and geometric calibration of CCD-cameras." *ISPRS J. of Photogrammetry and Remote Sensing*, 45, 17–32.

Brown, D. C. (1968). "Advanced method for the calibration of metric cameras." *Final Rep., Part 1, U.S. Army Contract: DA-44-009-AMC-1457, (X)*, Engrg. Topographic Lab., Fort Belvoir, Va., Florida.

Brown, D. C. (1971). "Close-range camera calibration." *Photogrammetric Engrg.*, 37(8), 855–866.

Curry, S., and Baumrind, S. (1986). "Calibration of an array camera." *Photogrammetric Engrg. and Remote Sensing*, 52(5), 627–636.

El-Hakim, S. F. (1986). "Real-time image metrology using CCD cameras." *Photogrammetric Engrg. and Remote Sensing*, Vol. 52, 1757–1766.

El-Hakim, S. F., Burner, A. W., and Real, R. R. (1989). "Video technology and real-time photogrammetry." *Non-topographic photogrammetry*, 2nd Ed., Am. Soc. of Photogrammetry and Remote Sensing, Falls Church, Va., 279–304.

Faig, W. (1972). "Design, construction and geodetic coordination of a close-range test field." *Civ. Engrg. Studies, Photogrammetric Ser. No. 32*, Univ. of Illinois, Urbana, Ill.

Faig, W. (1975). "Calibration of close-range photogrammetric system: mathematical formulation." *Photogrammetric Engrg. and Remote Sensing*, 41(12), 1479–1486.

Faig, W., and Owolabi, K. (1988). "The effect of image points density on photo-variant and photo-invariant bundle adjustment." *ISPRS*, Vol. 27, Part B5.

Fraser, C. S., and Veress, S. A. (1980). "Self-calibration of a fixed-frame multiple-camera system." *Photogrammetric Engrg. and Remote Sensing*, 46(11), 1439–1445.

Fryer, J. G. (1989). "Camera calibration in non-topographic photogrammetry." *Non-topographic photogrammetry*, 2nd Ed., Am. Soc. for Photogrammetry and Remote Sensing, Falls Church, Va., 59–70.

Ke, Y. (1995). "3-D surface mapping with computer vision," PhD dissertation, Univ. of Illinois at Urbana-Champaign, Urbana, Ill.

Kenefick, J. F., Gyer, M. S., and Harp, B. F. (1972). "Analytical self-calibration." *Photogrammetric Engrg.*, 38(11), 1117–1126.

Merchant, D. C., and Tudhope, R. L. (1989). "Aerial photo system calibration over flat terrain." *Photogrammetry and Remote Sensing*, 55(12), 1755–1763.

Obaidat, M. T. M. (1994). "Video metrology for documentation of engineering construction," PhD dissertation, Univ. of Illinois at Urbana-Champaign, Urbana, Ill.

Wiley, A. G. (1991). "Metric aspect of zoom vision," PhD dissertation, Univ. of Illinois at Urbana-Champaign, Urbana, Ill.

Wiley, A. G., and Wong, K. W. (1992). "Geometric calibration of zoom lenses for computer vision metrology." *Proc., 29th Int. Congr. of Photogrammetry and Remote Sensing*, Commission V, Int. Archives of Photogrammetry and Remote Sensing, Int. Soc. of Photogrammetry and Remote Sensing (ISPRS), Washington, D.C., 587–593.
Wolf, P. R., and Loomer, S. A. (1975). "Calibration of non-metric cameras." *Proc., ASP Symp. on Close-Range Photogrammetry Sys.*, Urbana, Ill., 373–393.
Wong, K. W. (1980). "Basic mathematics of photogrammetry." *Manual of photogrammetry*, 4th Ed., Am. Soc. of Photogrammetry, Falls Church, Va., 37–102.
Wong, K. W., and Obaidat, M. T. (1992). "DRSTEREO—a stereo measurement system for the PC." *Proc., Tech. Papers of the ASPRS/ACSM/RT 92 Meeting*, Am. Soc. for Photogrammetry and Remote Sensing (ASPRS) and Am. Congr. on Surv. and Mapping (ACSM), Bethesda, Md., 228–234.

APPENDIX II. NOTATION

The following symbols are used in this paper:

A = coefficient represents the point where the plane intersects the X-axis;
$\bar{\mathbf{A}}$ = residuals coefficient matrix;
B = coefficient represents the point where the plane intersects the Y-axis;
$\bar{\mathbf{B}}$ = corrections coefficient matrix;
C = coefficient represents the point where the plane intersects the Z-axis;
D = distance;
f = camera focal length;
k = affine scaling factor;
l_1, l_2 = radial distortion parameters;
m_{11}–m_{33} = rotation matrix elements;
p_1, p_2, p_3 = decentering distortion parameters;
$\mathbf{V}$ = residual matrix;
$\mathbf{W}$ = weight matrix;
X = X-axis coordinate of ground coordinate system;
X_j = X-axis coordinate of ground coordinate system of ground point j;
X_i^c = X-axis coordinate of ground coordinate system for exposure center (c) of photo i;
Y = Y-axis coordinate of ground coordinate system;
Y_j = Y-axis coordinate of ground coordinate system of ground point j;
Y_i^c = Y-axis coordinate of ground coordinate system for exposure center (c) of photo i;
Z = Z-axis coordinate of ground coordinate system;
Z_j = Z-axis coordinate of ground coordinate system of ground point j;
Z_i^c = Z-axis coordinate of ground coordinate system for exposure center (c) of photo i;
x_{ij} = x-axis coordinate (in the image domain) of image point j at photo i;
y_{ij} = y-axis coordinate (in the image domain) of image point j at photo i;

x_p = x-coordinate of the principal point;
y_p = y-coordinate of the principal point;
Δ = corrections matrix;
Δx_{ij} = correction of image coordinate in the x-axis;
Δy_{ij} = correction of image coordinate in the y-axis;
ε = discrepancy matrix;
κ = rotation angle around z-axis of the image (l and r are subscripts for left and right images, respectively);
λ_{ij} = scale factor at image point j of photo i;
ϕ = rotation angle around y-axis of the image (l and r are subscripts for left and right images, respectively); and
ω = rotation angle around x-axis of the image (l and r are subscripts for left and right images, respectively).